Portable Electromagnetic Induction Sensor with Integrated Positioning

MR-1712

Interim Report

Submitted to

Strategic Environmental Research and Development Program (SERDP)

April 16, 2012

Revision **1.1**

By

U.S. Army Corps of Engineers Research and Development Center
Cold Regions Research and Engineering Laboratory (CRREL)
72 Lyme Road
Hanover, NH 03755

Principal Investigators
Drs. Ben Barrowes, David George, and Fridon Shubitidze
benjamin.e.barrowes@usace.army.mil

This report was prepared under contract to the Department of Defense Strategic Environmental Research and Development Program (SERDP). The publication of this report does not indicate endorsement by the Department of Defense, nor should the contents be construed as reflecting the official policy or position of the Department of Defense. Reference herein to any specific commercial product, process, or service by trade name, trademark, manufacturer, or otherwise, does not necessarily constitute or imply its endorsement, recommendation, or favoring by the Department of Defense.

Contents

1 Abstract **ii**

2 Objectives **1**

3 Technical Approach **4**
3.1 Background 4
3.2 Pedemis Design 5
3.2.a Pedemis Tx Array 6
3.2.b Pedemis Rx Array 11
3.2.c Pedemis Control Electronics 13
3.3 Pedemis Rx Positioning 14
3.4 Background Subtraction 20
3.5 Pedemis Operation Protocol 21

4 Results and Discussion **22**
4.1 Pedemis Hardware and Fabrication 22
4.2 Pedemis DAQ Control Software 23
4.3 Initial Data, November 2011 23

5 Conclusions to Date **29**

References **30**

1 Abstract

SERDP project MR-1712 entitled "Portable Electromagnetic Induction Sensor with Integrated Positioning" is slightly more than halfway complete. The transmitter (Tx) and receiver (Rx) assemblies are designed and fabricated. The data acquisition (DAQ) electronics consists of the National Instruments (NI) cRIO platform which is much lighter and more efficient that prior DAQ platforms. Software to control the cRIO DAQ process has been written in NI's LabVIEW. This software has been used to successfully acquire initial data. Inversion of the data acquired during these initial tests has yielded satisfactory polarizabilities of a spherical target. In addition, precise positioning of the Rx assembly has been achieved via position inversion algorithms based solely on the data acquired from the receivers during the "on-time" of the primary field.

Major tasks still to complete include redesigning and integrating new transmitter and filter board control circuitry as well as final cable construction and integration. The LabVIEW programs must also be matured to become more user friendly. A more extensive prove-out is scheduled for May, 2012 after which will follow an extensive data analysis. Finally, we intend to go to Aberdeen Proving Ground in the Fall of 2012 to perform a field test of Pedemis, test its protocols, and evaluate its performance.

List of Acronyms (and page references to first use)

BUD	Berkeley UXO Discriminator – first used on page (4)
CRREL	Cold Regions Research and Engineering Lab – first used on page (1)
DAQ	Data AcQuisition – first used on page (ii)
EMI	Electromagnetic Induction – first used on page (1)
ERDC	Engineering Research and Development Center – first used on page (1)
ESTCP	Environmental Security Technology Certification Program – first used on page (5)
FPGA	Field Programmable Gate Array – first used on page (23)
JD	Joint Diagonalization – first used on page (3)
MAS	Method of Auxiliary Sources – first used on page (10)
MPV	Man-Portable Vector (subject of this final report) – first used on page (1)
MR	Munitions Response – first used on page (ii)
NI	National Instruments – first used on page (ii)
NSMS	Normalized Surface Magnetic Source – first used on page (3)
ONVMS	ortho-normalized volume magnetic source – first used on page (3)
Pedemis	PortablE Decoupled Electromagnetic Induction Sensor – first used on page (ii)
RMS	Root Mean Squared – first used on page (5)
RT	Real Time – first used on page (23)
Rx	Receiver – first used on page (ii)
SERDP	Strategic Environmental Research and Development Program – first used on page (ii)
SNR	Signal-to-noise ratio – first used on page (5)
TEMTADS	Time domain ElectroMagnetic Towed Array Detection System – first used on page (1)
Tx	Transmitter – first used on page (ii)
USACE	United States Army Corps of Engineers – first used on page (1)
VI	Virtual Instruments – first used on page (23)

Keywords: electromagnetic induction, handheld, time domain, rigorous models, inversion

Acknowledgments: This project was funded by the Strategic Environmental Research and Development Program (SERDP) under project MR-1712. We worked closely with G&G Sciences and Dartmouth College for the duration of the project. Drs. Jeff Marqusee, Anne Andrews, and Herb Nelson, and the review committee for SERDP, provided support and constructive reviews during the course of the project.

List of Figures

2.1 Conceptual design of the proposed sensor. 2
3.1 Examples of challenging terrain for which Pedemis could be deployed. 4
3.2 Pedemis Tx array 6
3.3 Pedemis Rx array 7
3.4 Pedemis control electronics 8
3.5 Possible design of Tx array. 9
3.6 Simulated 2x2 Tx array results 10
3.7 Simulated 3x3 + 4vertical Tx array results 11
3.8 Simulated 3x3 Tx array results 12
3.9 Pedemis receiver cubes 13
3.10 Pedemis control electronics 14
3.11 Pedemis beacon example 16
3.12 Pedemis beacon example error 17
3.13 Pedemis beacon target induced error 17
3.14 Pedemis Beacon Inversion #1 18
3.15 Pedemis Beacon Inversion #2 19
3.16 Pedemis DAQ Position #1 22
4.1 Pedemis RT control software 24
4.2 Pedemis FPGA control software 25
4.3 Initial Data Setup 26
4.4 Example data from Pedemis 27
4.5 Polarizabilities from data in Fig. 4.4. 28

List of Tables

2 Objectives

The objective of this work is to design and fabricate a novel time-domain bistatic EMI sensor that allows for the physical decoupling of the transmitter (Tx) and receiver (Rx) coil(s). This bistatic, physically decoupled, portable EMI instrument with precise positioning would be a valuable research instrument for several reasons. First, there is a pressing need for portable EMI instruments deployable in adverse conditions where cart mounted systems cannot function. Furthermore, a bistatic EMI instrument also delivers critical flexibility in operation and high fidelity data by allowing users to acquire sufficiently detailed data in one pass to satisfy inversion/discrimination routines (see Sec. 3.5). Necessary in achieving this data quality is research into a more precise scheme for positioning the receiver assembly. We will to combine systematic modeling of the instrument geometry, flexible operation design, and highly precise positioning into a single, portable EMI instrument.

This bistatic configuration allows greater positioning accuracy, improved depth detection, deployment flexibility, and deployment in difficult terrain. This sensor will have a built-in precise positioning system, can be operated in either a carted or man-portable mode, and features an array of vector (coil) receivers. Figure 2.1 provides a sketch of the proposed design. In summary, the sensor will consist of a movable coplanar set of transmitting coils, a movable detachable array of receiver coils, and supporting hardware (e.g. in a backpack, see see Sec. 3.2). The system can be used in either a bistatic mode, i.e. with Tx and Rx physically decoupled; or in a monostatic mode (Tx and Rx in a fixed geometry). Subcentimeter or even submillimeter positioning of the receivers will be a design goal via receiver cube detection of the primary field during the "on" time of the transmitter (see Sec. 3.3). Transmitter and receiver geometries and characteristics were rigorously modeled in an effort to systematically determine optimal instrument configurations (see Sec. 3.2).

The specific objectives of this project are:

1. **Modeling of physically decoupled EMI instrument configurations (see Sec. 3.2)**
   This will be a bistatic instrument with the Tx and Rx coils physically decoupled and separately movable. This decoupling allows simpler data processing for some algorithms, while suimultaneously allowing multiple operational modes (see Sec. 3.2), but will require precise positioning (see Sec. 3.3). The number, geometry, and arrangement of both the transmitters and receivers will be rigorously modeled and investigated with tools from prior SERDP projects for maximum data information given hardware constraints. The receivers will be dB/dt vector coil receivers with a lighter core than those of the MPV (MR1443).
2. **Versatile instrument with multiple operational modes**
   This instrument has two separate components: a square planar transmitting array consisting of nine coplanar 40cm TEMTADS size Tx coils, and a detachable 3x3 array of vector receivers which can be either placed to collect static data or moved around above the transmitting coils to obtain dynamic data (see Fig. 2.1). Both of these components can be affixed to a cart for larger scale detection surveys, or can be dismounted from the cart and carried by two people in a gurney like configuration for cued interrogation even in rugged and/or challenging terrain. For increased depth detection and possible noise reduction, an additional mode consisting of a stationary receiver assembly and multiple transmitter positions will be investigated. In summary, the following operational modes will be considered and evaluated during this project:

   (a) Carted Mode (relative geometry fixed)

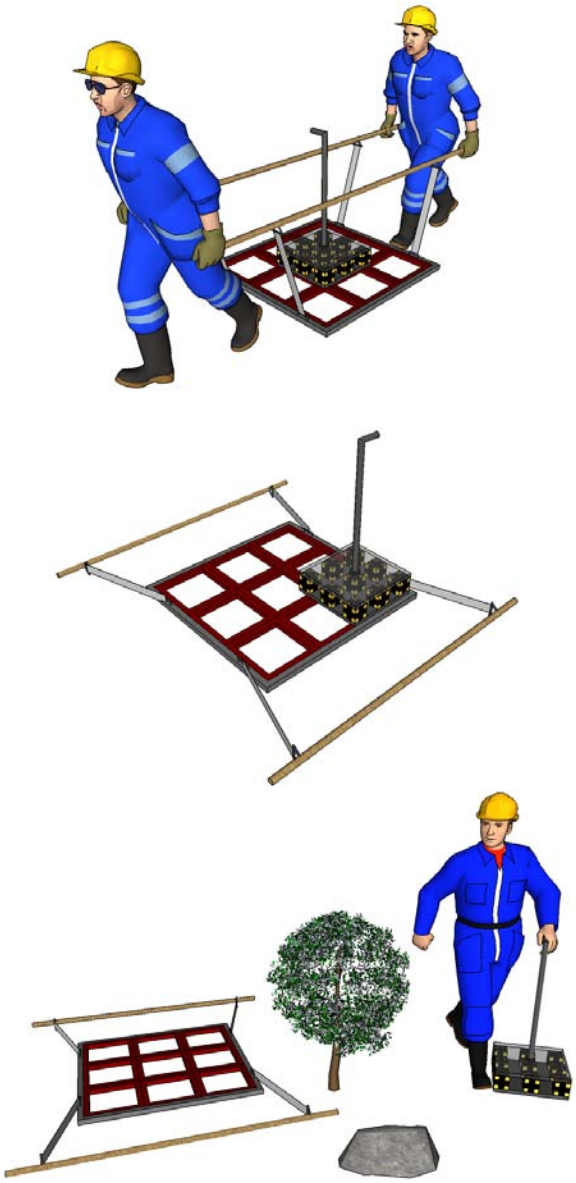

Figure 2.1: Conceptual design of the proposed sensor. Flexible modes of operation allow either cart mounted or man portable operation, static or dynamic data acquisition. This bistatic configuration allows greater positioning accuracy, improved depth detection, and deployment in difficult terrain. The nine red squares correspond to the Tx coils, while the receiver array is located on top of the Tx coils in the top figure.

(b) Cued Interrogation Mode (receivers detached, transmitters stationary [with or without cart])
(c) Man-Portable Detection Mode
(d) Superposition Mode (receivers stationary, transmitters moved around)

3. **Integrated positioning system (see Sec. 3.3)**
   To use data from bistatic instruments, the local position of the sensor must be known with as high precision as possible. To this end, a novel beacon positioning system will be implemented into this instrument with the goal of attaining subcentimeter (possibly submillimeter)

level positioning of the receiver coil assembly relative to the transmitters. The receivers will detect the primary magnetic field during the "on" time of the (stationary) transmitter. Combining and averaging the data from each of the transmitters will allow precise positioning of the receiver cubes by detecting the powerful and well known primary fields. These same receiver cubes will then collect EMI data during the transmitter "off" time.

This multimode bistatic portable array instrument, called Pedemis (PortablE Decoupled Electromagnetic Induction System), will fulfill these objectives based on research into the optimal size, constitution, and configuration of transmitters, receivers, and supporting hardware while also incorporating several improvements over existing sensors (Sec. 3.2). This new positioning method will add to the information content of the data, allowing more accurate inversions, without adding any hardware to the instrument itself. We will incorporate instrument control software which can deliver some feedback to the operator regarding targets in real time (see Sec. 4.2). As well, the flexible operation of this instrument will allow deployment in both cart-trafficable sites and more challenging sites.

Standard models such as the dipole model [1] and more rigorous models such as the Joint Diagonalization (JD) method [2], Orthonormalized Volume Magnetic Source Method (ONVMS) [3, 4], NSMC [5–13], and analytical models [14–20] will be applied to the data acquired from this instrument (Sec. 4.3). These models, in tandem with the diverse, extremely high quality data from this instrument will result in more accurate discrimination capability and fewer false alarms.

The new Pedemis instrument is designed to attack successfully the task of close interrogation of signal anomalies, for discriminating UXO from clutter, in non-trafficable, rugged terrain.

3 Technical Approach

3.1 Background

The detection and discrimination of UXO depend on both realistic and rigorous modeling and high-quality, diverse data. Recently, several new electromagnetic induction (EMI) sensors have been developed including TEMTADS (MR-0601, MR-1315), MetalMapper (MR-0603), BUD (MR-0437), Geometrics integrated magnetometers (MR-1512), and our MPV (MR-1443 continued in MR-201005) and GEM-3$\mathscr{D}^+$(MR-1537). These sensors represent the state of the art in the electromagnetic induction sensing. However, there is still significant room for improvement. For example, most of the recent sensors are cart based systems meant for rapid surveying of sites with benign terrain. As a result, the geometry of the sensor is fixed, which limits data diversity by limiting the collection of data at only fixed location(s) above a target. Inversion modeling is then based on a few data points and a limited look at each anomaly. If additional data points (i.e. different transmitter locations) are used in modeling an anomaly, geolocationing between data points becomes critical but is limited in accuracy by the geolocationing system itself and cart motion. In addition, if there are multiple targets (counting clutter) in the field of view of the sensor, the limited data collected at one location may not be sufficient to resolve multiple targets. Moreover, these carted sensors cannot be deployed at treed sites or sites with challenging terrain (see e.g. Fig. 3.1).

Figure 3.1: Examples of challenging terrain for which Pedemis could be deployed.

Recent man-portable sensors include the MPV [21, 22], GEM-3$\mathscr{D}^+$and the "mini-TEMTADS". The MPV shows promise with its five vector receivers, large sensor head, excellent SNR, and good depth of detection. With it we have been able to show excellent discrimination results at the Camp Beale ESTCP demonstration site. Even with these encouraging results, the MPV has shown some weaknesses in the areas of positioning, data acquisition modes, and physical design. The beacon positioning system conceived in ESTCP MR-0738 and implemented in the new MPV2 is simpler to operate and will work in treed and challenging sites. However, this positioning system adds to the overall complexity of the instrument, adds time to data acquisition procedures, and currently at best provides only 1 cm RMS positioning error. For high fidelity modeling and operational issues, a more accurate and less complicated positioning scheme is desired. Here we make the distinction between positioning, or knowing the position of the Rx coils locally relative to the Tx coil, and geolocationing, or knowing where the sensor is globally (using using e.g. GPS or RF).

All of the above mentioned sensors are monostatic or multistatic with the transmitter coil(s) either collocated with or physically attached to the receiver coils. While there are some advantages to this arrangement (not the least of which is ease of design), data from monostatic sensors are more difficult to model for some algorithms (e.g. upward continuation techniques from MR1590). The user is also typically forced into choosing either a carted sensor and its ability to stop and acquire a few high SNR data points, or a handheld sensor and its forte of acquiring copious data as it is dynamically moved about. A sensor which combines both operational modes would be a significant improvement over these existing sensors. In addition, in multi-static deployment of this proposed sensor, because the Rx coils are movable with respect to the Tx coils, various operational modes which reduce noise and increase data quality are possible (see Sec. 4.3). Our Rx coil array also has the ability to acquire spatial tensor gradients of the magnetic field which help in finding the location of dipolar sources [23, 24] (see Sec. 4.3).

3.2 Pedemis Design

The Pedemis hardware can be considered in three major parts:

1. Tx array
2. Rx array
3. Controlling electronics

The following sections will describe the design considerations of each of these three aspects of the instrument. As we designed Pedemis, we kept in mind the following design objectives:

1. maintain physical decoupling of Tx and Rx arrays (see Sec. 3.2.a and Sec. 3.2.b)
2. high SNR data
3. the target should be illuminated from multiple look angles (see Sec. 3.2.a)
4. Tx weight plus Rx weight remain under 45 pounds (see below)
5. 2 minute or less primary data collection sequence (excludes a follow up interrogation for suspected deep targets, see Sec. 3.5)
6. controlling electronics be lighter weight than previous instruments (see Sec. 4.2)

7. flexible, simple, and robust user interface (see Sec. 4.2)
8. at most, two people required to operate
9. subcentimeter positioning of the Rx array (see Sec. 3.3)
10. be able to apply our advanced models at both the data acquisition stage and post processing stage

As of January, 2012, the Tx and Rx arrays have been fabricated as shown in Figs. 3.2–3.4.

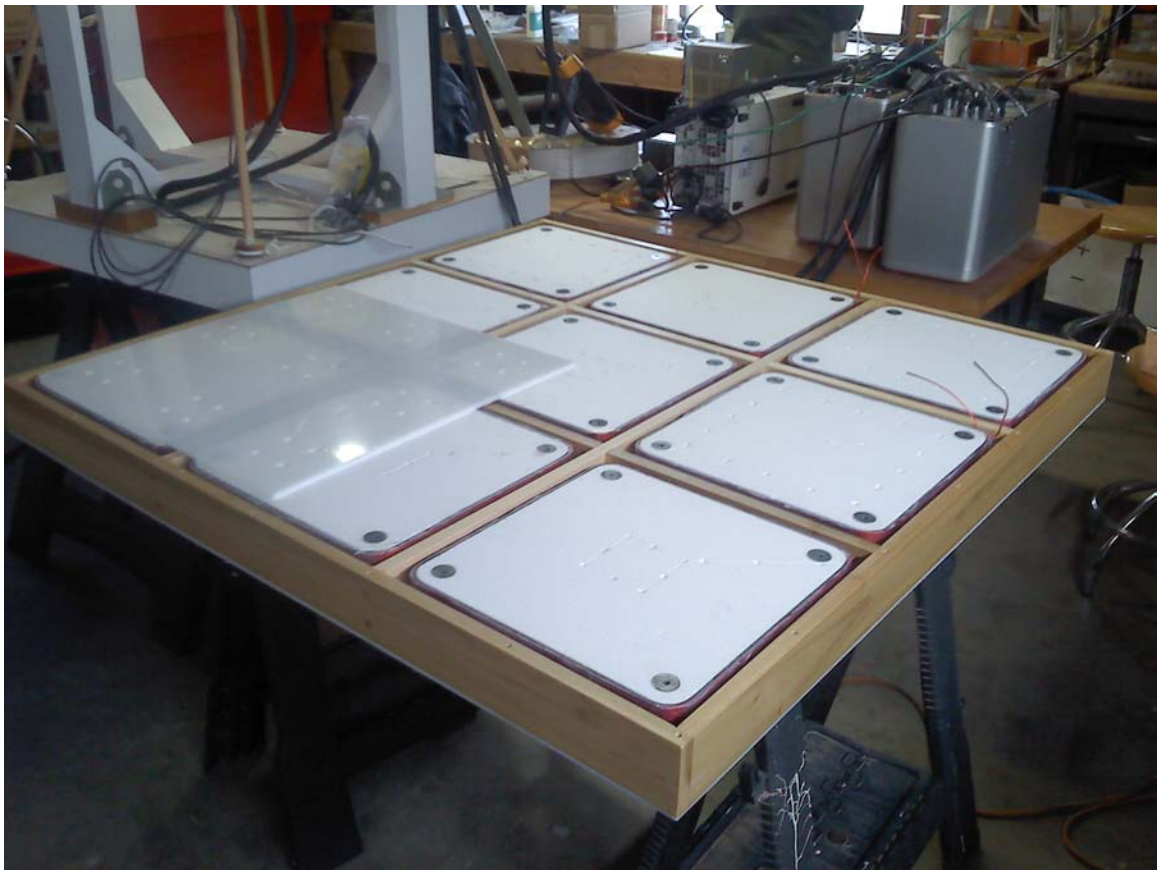

Figure 3.2: Pedemis Tx array. Tx loops are the same size and template as the TEMTADS coils. 35cm loop size with 40cm between centers. See Sec. 3.2.a for more information about the Pedemis transmitter array.

The combined weight of these arrays is about 38 pounds which does not include cabling or gurney poles. The Tx array is 1.2 meters on a side, while the Rx array is 50cm on a side. The overall weight of the controlling electronics (NI cRIO) plus batteries is approximately 20 pounds. The mostly fabricated Pedemis instrument described herein fulfills the above design goals, resulting in an advanced and effective EMI instrument capable of acquiring high quality data from a flexible platform.

3.2.a Pedemis Tx Array

We considered various designs for the Pedemis Tx array. Here is a list of the designs considered:

Figure 3.3: Pedemis Rx array on top of the Tx array. Rx receiver coils are the same size and template as the MPV2 coils. Receiver coils have an 8cm loop size with 20cm between centers. See Sec. 3.2.b for more information about the Pedemis receiver array.

1. 4 or 9 horizontal coplanar coils
2. 4 vertical side coils or not
3. 1 large encompassing coil or not

Together there were 8 possible base configurations not counting sizing of the coils. Figure 3.5 shows some possibilities we considered during the design phase of Pedemis.

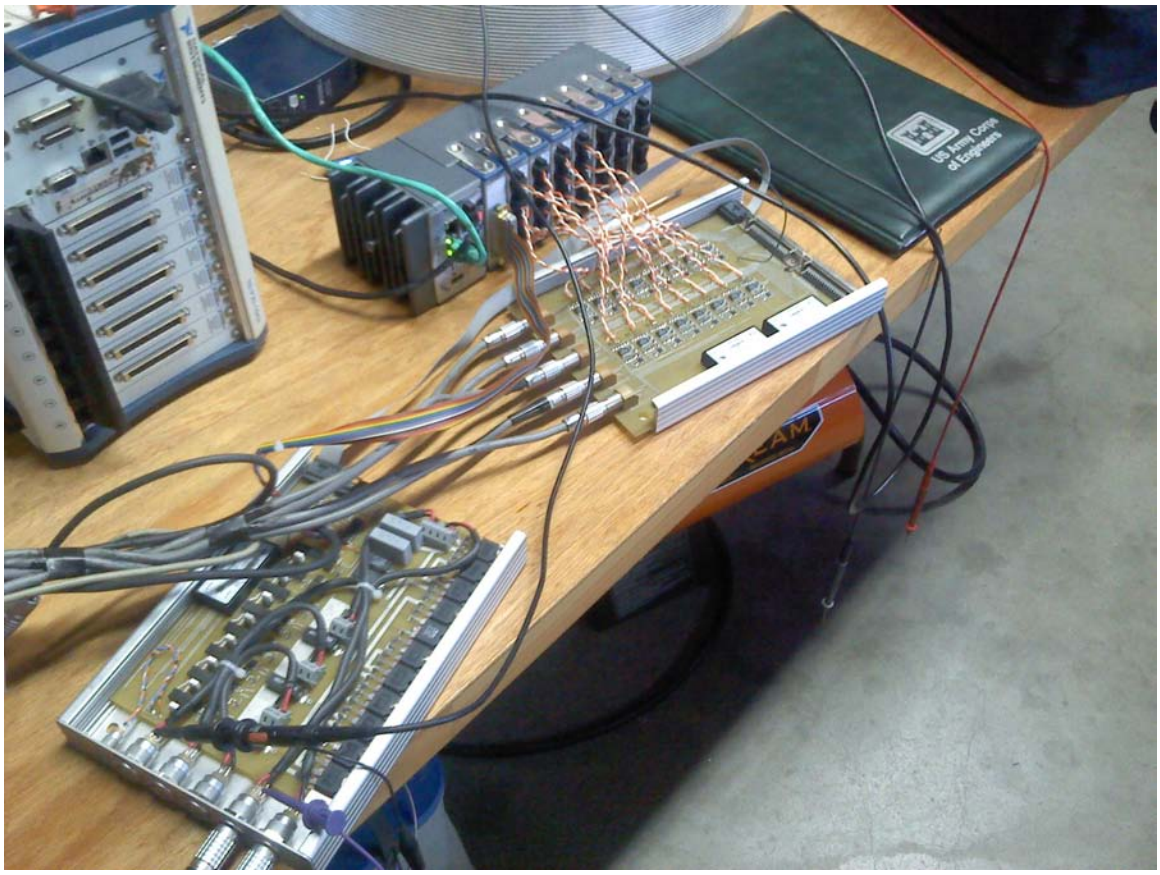

Figure 3.4: Pedemis control electronics. A National Instruments cRIO system with DAQ modules and a digital IO module control Pedemis's transmitters and receivers. See Sec. 3.2.c for more on the electronic control system of Pedemis. The cRIO is programmed in LabVIEW (see Sec. 4.2 for more on Pedemis control software). Also shown are the old transmitter control board (lower left) and the old filter board (in front of cRIO). For more on these electronics, see Sec. 4.1.

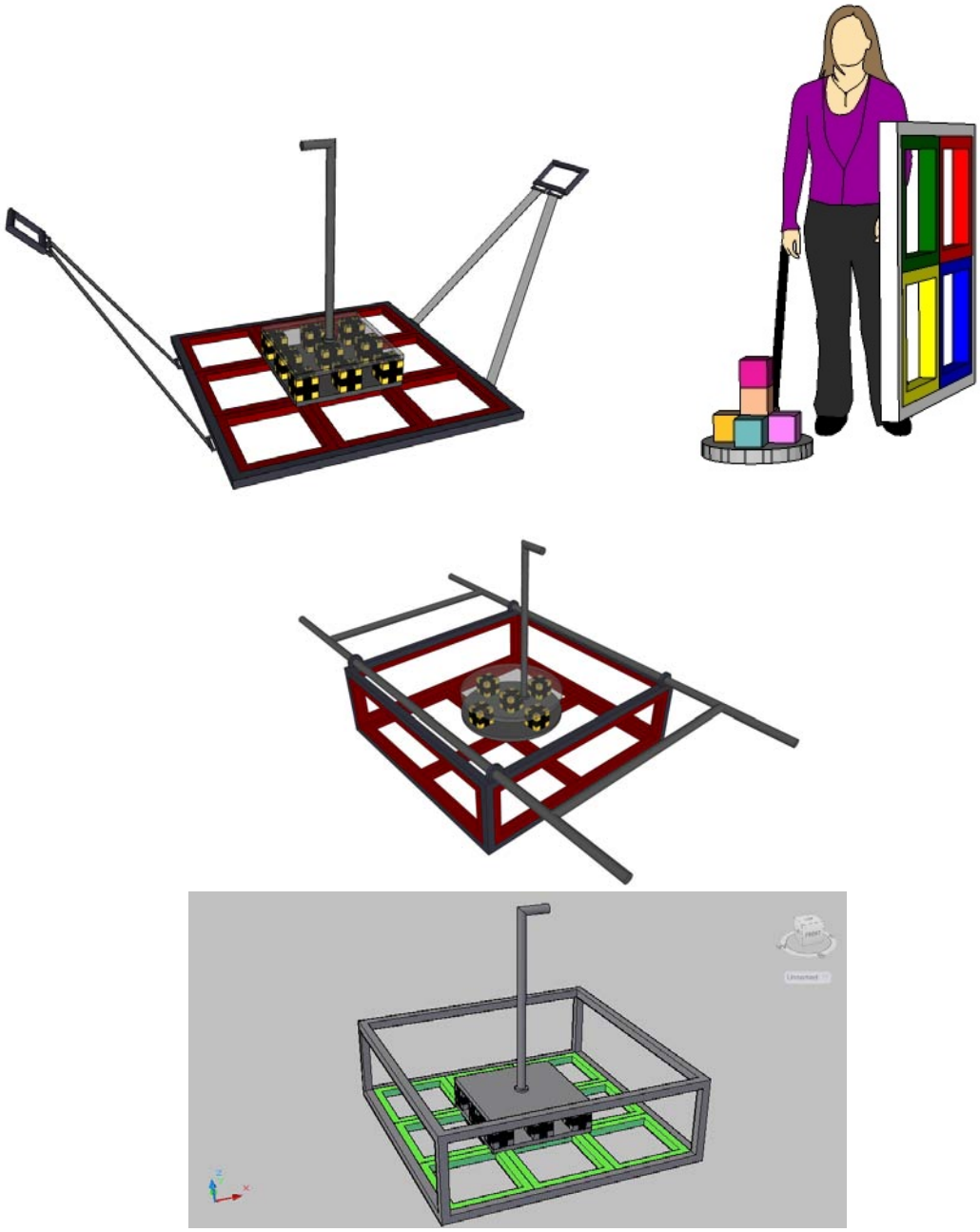

Figure 3.5: Possible designs of Tx and Rx arrays considered during the design phase of Pedemis before arriving at the design in Fig. 2.1.

We simulated various designs for the Pedemis transmitters to help us decide which Tx configuration would best achieve the design goals in Sec. 3.2. Figures 3.6–3.8 present the results of three simulations illustrating the trade offs associated with different numbers of coils with different sizes in different configurations. All three figures show the inverted total ONVMS from a 60mm mortar at 40cm depth to center simulated with the MAS (method of auxiliary sources) algorithm. The straight line shows the result without noise added to the secondary field, while the line with circles shows the inverted result with some noise added to the synthetic data.

Figure 3.6 shows that for a 2x2 Tx array, while the algorithm was able to invert for the T-ONVMS, the results degraded quickly for the amount of noise added with the result that the T-ONVMS with noise is significantly different than the T-ONVMS without noise even at early time where the secondary field is the strongest. This is due to the target being illuminated by only 4 look angles with this 4 Tx configuration. The amount of information at the receivers about the target is less than with a configuration that has more transmitters. For anomalies with multiple targets present, fewer transmitters also results in a lessened capability to discriminate between the various targets due to a lack of information.

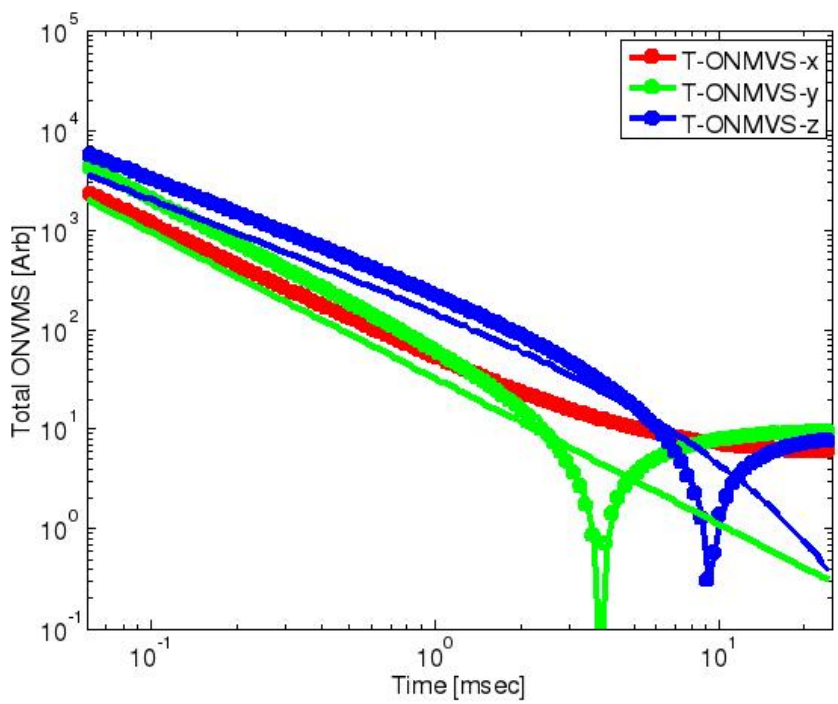

Figure 3.6: Simulated 2x2 Tx array results. Tx loop size was 45cm on a side. The lines without circles show the result without noise added, while the lines with circles shows the inverted result with some noise added to the synthetic data.

On the other hand, as can be seen in Fig. 3.7, when there are more Tx with some Tx in a vertical orientation, the inverted T-ONVMS for noisy synthetic data follows the noise free T-ONVMS to a much later time due to the many more look angles and increased information in the data. The four added vertical coils do help some in interrogating the anomaly, but also unfortunately add considerable weight to the assembly via their metal weight and necessary supporting structure.

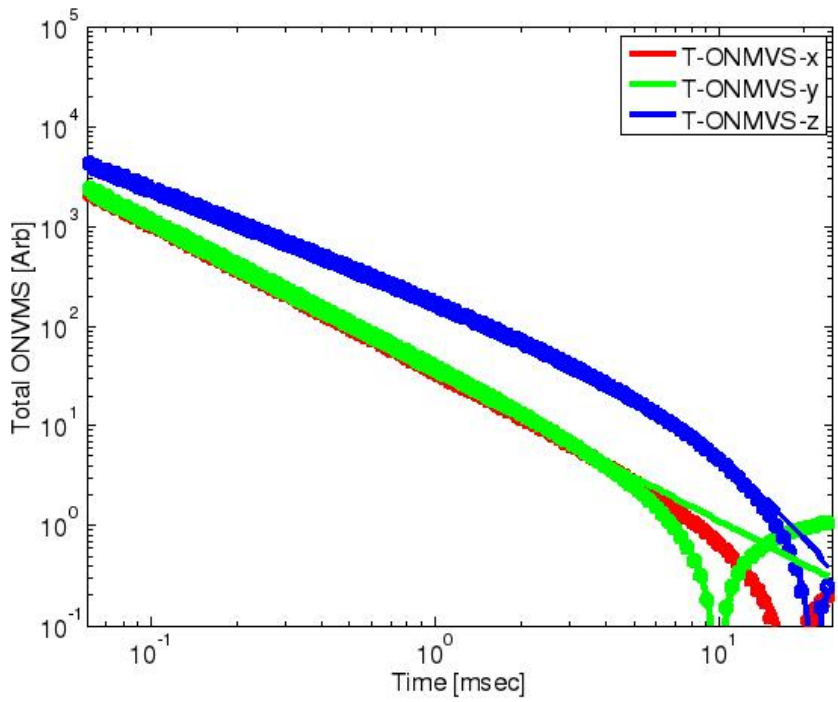

Figure 3.7: Simulated 3x3 + 4vertical Tx array results. Horizontal Tx loop size was 30cm on a side. Vertical Tx loop size was 30cm tall 90cm long. The lines without circles show the result without noise added, while the lines with circles shows the inverted result with some noise added to the synthetic data.

In between these two extremes is the 3x3 array with results shown in Fig. 3.8. This configuration results in only minimally worse T-ONVMS for the noisy case than the case with the four vertical coils. The takeaway here is that while the four vertical coils can add information for the inversion algorithms, the added information is not significant, but the increase from a 2x2 to a 3x3 Tx array does add resolution and data diversity to the secondary field recorded by the receivers.

Given these considerations and the practical constraints imposed by Tx circuitry, weight, and complexity, we decided on a 3x3 Tx array with 35cm transmitters (same Tx design as TEMTADS) spaced 5 cm apart resulting in an overall Tx assembly of 1.2m on a side weighing about 35 pounds. This compromise yields high quality data with several looks at the anomaly sufficient to distinguish multiple targets in highly cluttered environments.

3.2.b Pedemis Rx Array

From a data analysis standpoint, more data from more receivers in an EMI system will lead to a more robust result. However, given practical considerations of size, weight, and cabling, only a finite number of receivers can be implemented. Experience with the MPV and MPV2 [21, 22] made it clear that vector receiver cubes which measure all three components on the secondary magnetic field from the target produced superior data than single axis receivers. As a result, one early decision was to use these 8cm receiver cubes in Pedemis (see Fig. 3.9). These cubes are made from 8cm balsa wood blanks routed to accept small diameter copper wire especially wound to produce the same receiver moment in all three dimensions. For more information on the design

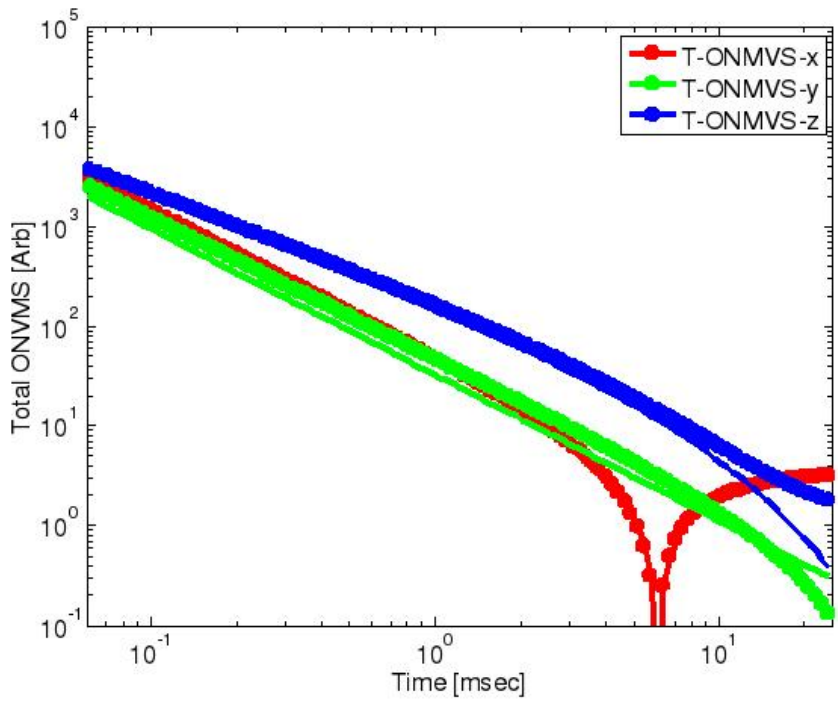

Figure 3.8: Simulated 3x3 Tx array results. Tx loop size was 30cm on a side. The lines without circles show the result without noise added, while the lines with circles shows the inverted result with some noise added to the synthetic data.

of these Rx cubes, see the MPV-II documentation.

The question of how many Rx cubes to implement on Pedemis involves many considerations including weight, complexity, number of DAQ modules in the NI cRIO, cabling issues, protocol (see Sec. 3.5), operator fatigue, etc. Each receiver cube requires an additional preamplifier board near the cube itself to minimize stray EM noise from the surroundings. Additionally, 9 separate wires and 3 DAQ channels are required to accommodate each cube. Originally, we considered a 6x6 stationary Rx array for Pedemis, but abandoned that due to practical considerations. Perhaps if a multiplexed Rx array were to be designed, then this number of Rx channels ($3 \times 36 = 108$) could be accommodated. Aside from these practical matters, we wanted the Rx array to be physically decoupled from the Tx array, so this fixed design was not implemented.

The 6x6 array of 20cm spaced secondary field samples was still desirable, however, so a compromise 3x3 array moved into the 4 corners on top of the Pedemis Tx array was suggested. The 20cm sampling size in our analysis is sufficient to discriminate between objects in close proximity without being redundant for most anomalies seen to date. Though the 3x3 array would require moving the Rx array 4 times for the most detailed data shot, the advantages of dense, high quality data while preserving a manageable cabling and DAQ module load outweighed the increase in complexity of the data acquisition protocol. This compromise also conveniently allowed the Rx array to be decoupled from the Tx array while keeping the weight to about 10 pounds. See Sec. 3.5 for more information on Pedemis deployment protocols. The position of the Rx array is calculated via measurements of the primary field during the "on" time of the Pedemis transmitters. For more on this positioning method, see Sec. 3.3.

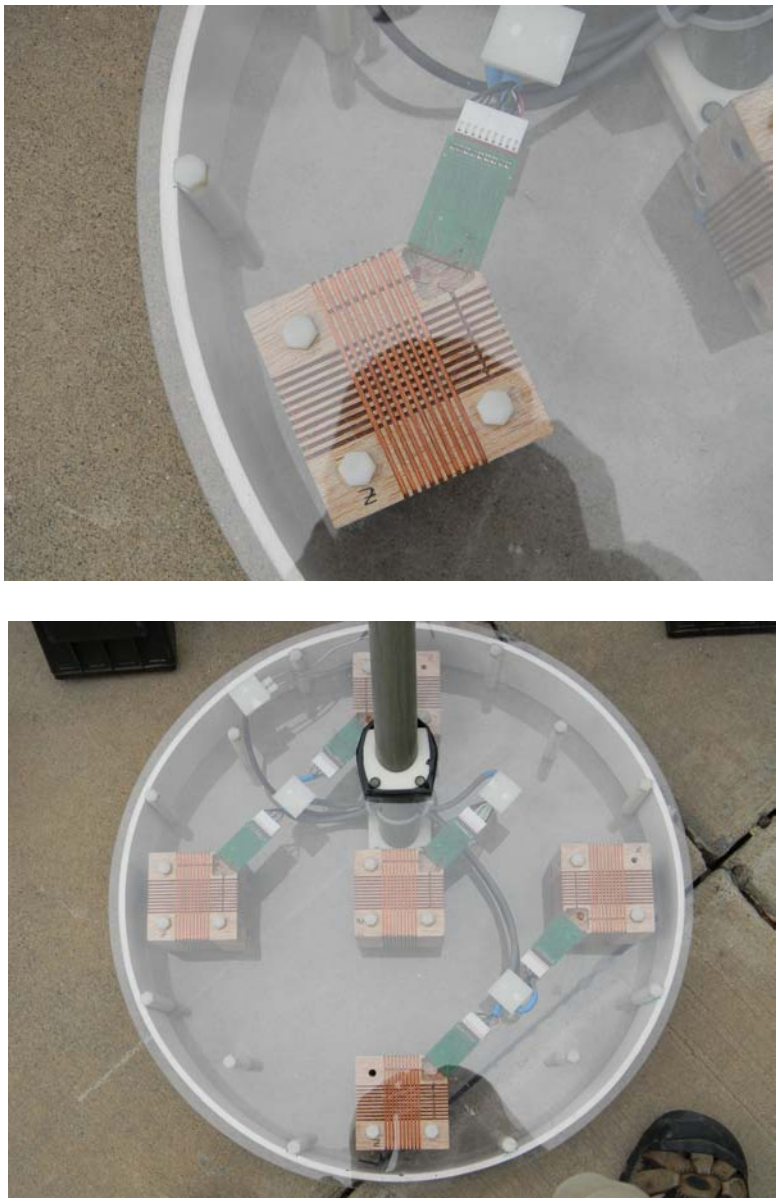

Figure 3.9: Receiver cubes from the MPV-II instrument also used in the new Pedemis. Cubes are made from 8cm balsa wood blanks routed to accept small diameter copper wire.

3.2.c Pedemis Control Electronics

Pedemis uses the NI cRIO for controlling the Tx and Rx arrays and associated circuitry. This represents a step forward from prior portable EMI systems like the MPV-II in terms of weight, power usage, and decreased complexity. The weight of the cRIO chassis and modules is around 8 pounds compared to over 20 for the full PXI chassis and related electronics. Instead of 3 lithium ion batteries and 3 hour swap intervals, we expect to use only 2 of these batteries with a 5-6 hour swap interval. Also, the cRIO chassis, with its integrated modules, is simpler and more robust than the prior full PXI chassis, but the cRIO is still a fully functioning field ready computing platform. There are 4 main components to the cRIO control system shown in Fig. 3.10 and Fig. 3.4:

1. CRIO-9022, Real-Time PowerPC Embedded Controller for CompactRIO, 533 MHz, 2 GB storage, 256 MB DRAM
2. cRIO-9116, 8-slot Virtex-5 LX 85 Reconfigurable Chassis for CompactRIO
3. NI 9222, 4-Ch, 10 V, 16-Bit, 500 kS/s, Simultaneous AI C Series Module for CompactDAQ and CompactRIO (Pedemis needs 7 of these: 27 Rx channels and 1 Tx current channel)
4. NI 9401 8-Channel, 100 ns, TTL Digital Input/Output Module

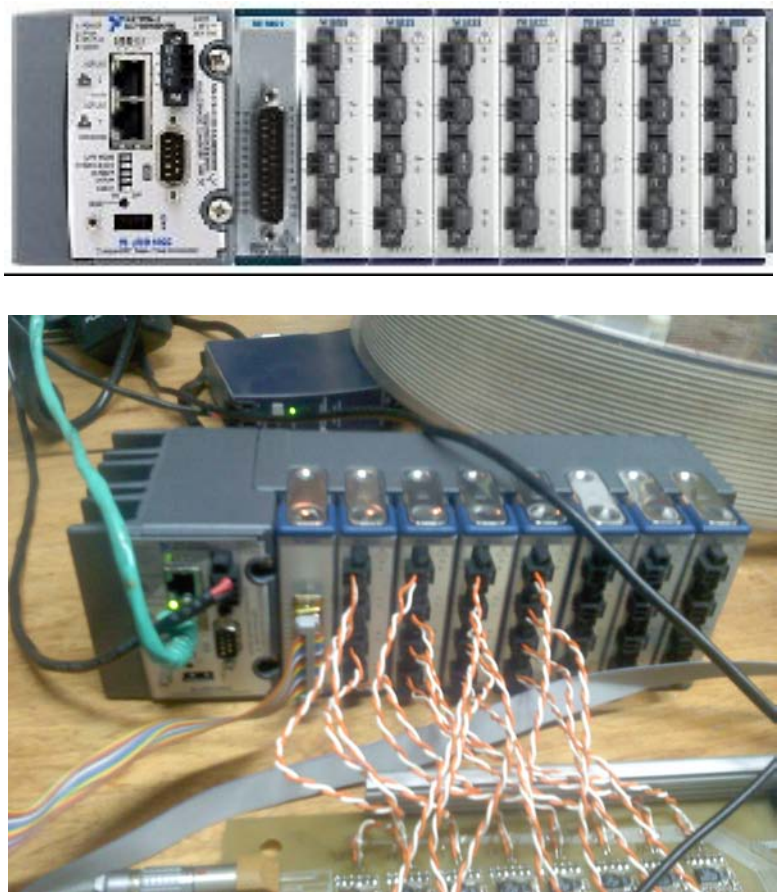

Figure 3.10: Pedemis control electronics. Upper figure is as designed at NI.com. Lower figure is as configured for the initial data reported in Sec. 4.3. The NI-9401 is in the leftmost slot while the 7 NI-9222's are in the remaining 7 slots of the 8 slot chassis.

The only current disadvantage to using the NI-cRIO platform is that G&G's EM3D control software written in Visual Basic and C# would not run on the cRIO, thus necessitating programming Pedemis control software in LabVIEW from scratch. We have made progress in programming this software, and this is discussed in more detail in Sec. 4.2.

3.3 Pedemis Rx Positioning

The Rx array on Pedemis is not held in a fixed geometry relative to the Tx array except as noted in Sec. 3.5 for cued interrogation mode #1. As a result, the position of the Rx array must be retrieved

in order for data shots taken at different Rx array positions to be be meaningful. This position of the Rx array is found on Pedemis by a beacon positioning approach, an approach first conceived in our MR-1537 GEM-3$\mathscr{D}^+$project and continued in MR-1443 MPV and MR-201005 MPV2.

The beacon positioning concept relies on the capability of the receivers to measure the strength of the primary field when each transmitter is being energized. After these data from the "on" time of the transmitter are recorded, the receivers then collect EMI data from the "off" time of the transmitters. Given these "on" time data, the geometry of the transmitters, and a record of the current in the energized transmitter, it is possible to calculate where the Rx array is in 3D space to under 1cm accuracy when the Rx array is within 2 meters of the Tx array.

We modeled the Pedemis beacon positioning system in order to predict how accurate we could expect the calculated position to be. Figure 3.11 shows an example of the Rx array above a model of the Tx array with the closest receiver at least 10cm away from the Tx coils. Using our simulation as a sanity check, if we use all four expected Rx array locations (as in cued interrogation mode #2, see Sec. 3.5), there is essentially only numerical error on the order of machine precision for the inverted position of the Rx array (see Fig. 3.12).

After these types of sanity checks, we also wanted to make sure targets under the Tx array would not distort the primary field sufficiently to degrade the "on" time measurements and produce a false position. To this end, we added a simulated 10cm sphere only 10cm below the center of the Tx array to see what effect it would have on the primary field and thereby the inverted Rx array position. Figure 3.13 shows the log10 positional error in the inverted Rx array location when the Rx array is 10cm above the Tx array and the sphere is present. Even though the presence of the sphere caused up to 1.5% perturbation of the primary field for some Tx/Rx combinations, the overall position of the Rx array was accurate to within less than 1mm.

We applied the algorithms developed during the simulation phase to the initial data collected in November 2011 in Grand Junction, CO (see Sec. 4.3). For the data shot #3 in Sec. 4.3, the MPV2 sensor head was left in one location (at the bottom right corner of the Tx array) while all nine transmitters fired in turn (see Fig. 4.3). For this case, with the Rx array directly over the (undamped) transmitters, the error in the inverted Rx array position was 2-3mm, which is on the order of our physical measurement expected error.

Our final test corresponding to data shot #4 in Sec. 4.3 tested whether the position of the Rx array could be inverted for even when the Rx array was positioned outside the Tx array (see Fig. 3.14). Figure 3.15 shows the inverted position of the Rx array using our algorithms. In this case as well, the inverted position was withing half a centimeter which is within the manual positioning and measurement error.

These results are encouraging in that they suggest that the beacon positioning system and algorithms can invert for the position of the Rx array when the Rx array is within a meter of the Tx array. The accuracy appears to be within 1cm and in most cases on the order of a few millimeters.

More details on the exact algorithms developed for Pedemis positioning will be included in the final report.

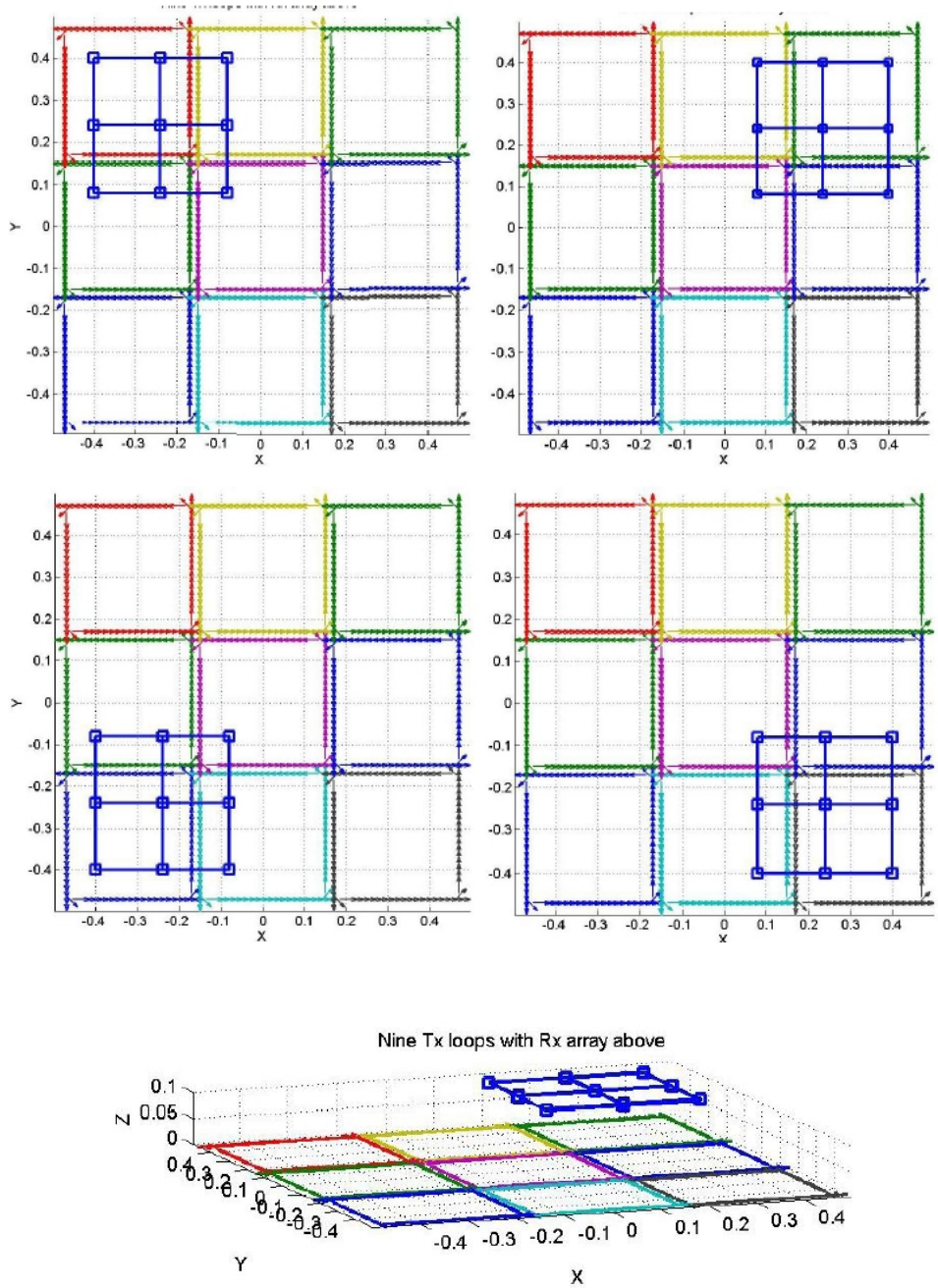

Figure 3.11: Pedemis beacon example with Rx array above the Tx array.

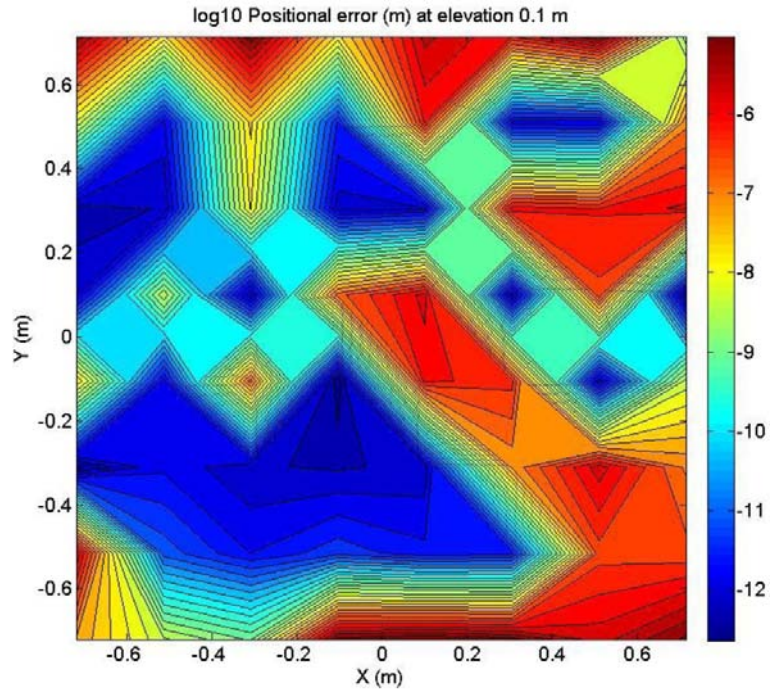

Figure 3.12: Pedemis beacon example error. For this synthetic case, the error is essentially only numerical error on the order of machine precision for the inverted position of the Rx array.

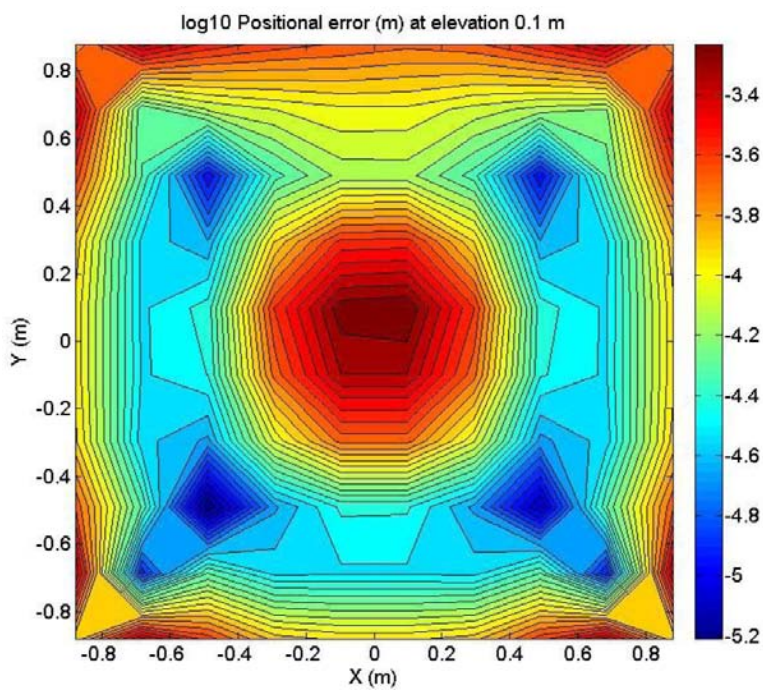

Figure 3.13: Pedemis beacon target induced error from a sphere placed under the Tx array.

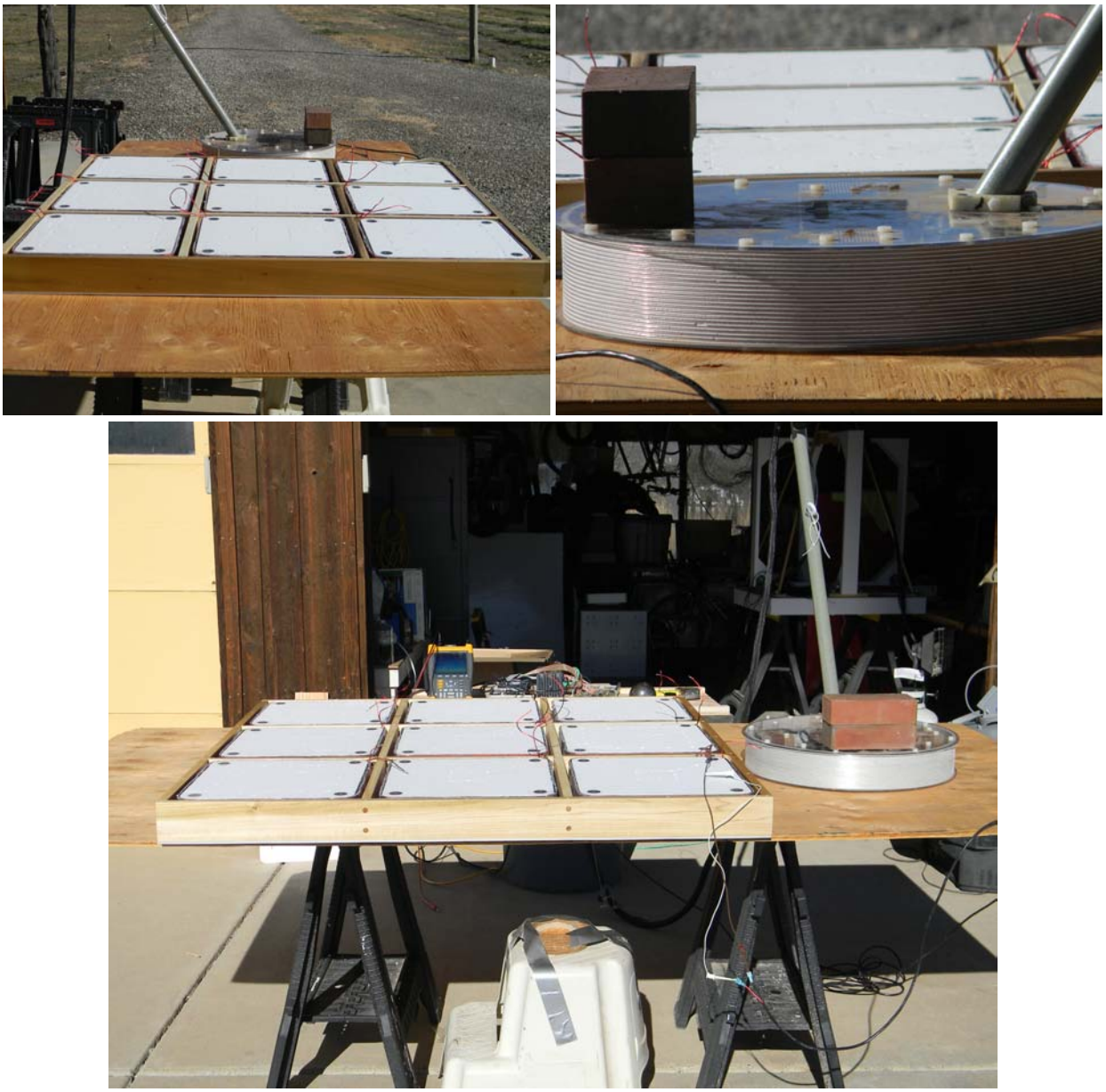

Figure 3.14: Pedemis Beacon Inversion #1 for the case of the MPV2 at the lower right hand corner of the Tx array. No target was present and the inverted position was within 0.5cm of the measured position.

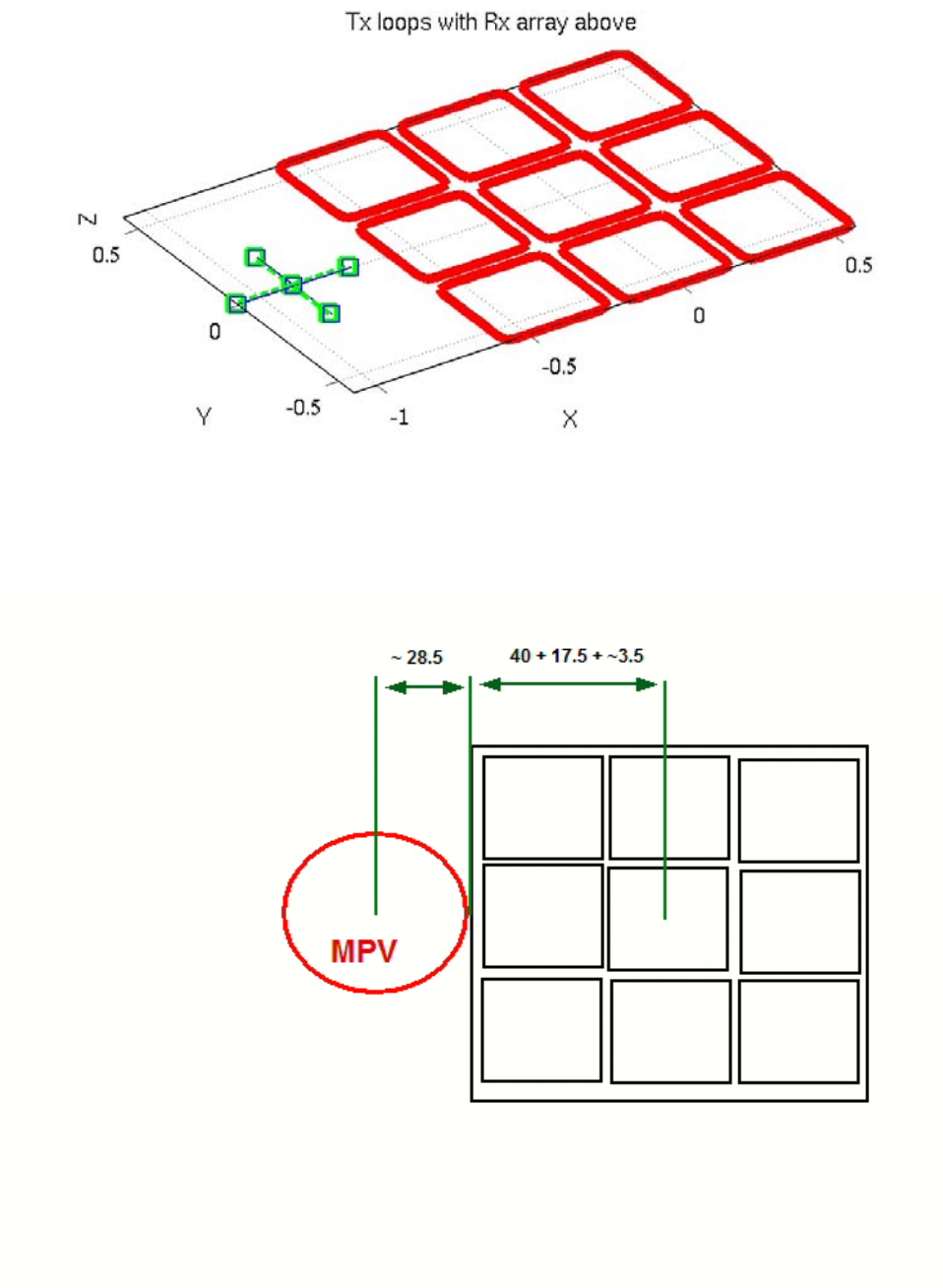

Figure 3.15: Pedemis Beacon Inversion #2 for the case of the MPV2 outside and to the left of the Tx array. No target was present and the inverted position was within 0.5cm of the measured position.

3.4 Background Subtraction

All EMI instruments generally have to account for background noise when acquiring data or the results may be poor or corrupted. With all prior EMI instruments, the transmitter(s) and receiver(s) have been in a fixed geometry with respect to each other, so acquiring a background shot was a relatively simple matter of finding a quiet location and acquiring a data shot. Because the Tx and Rx arrays on Pedemis are not in a fixed geometry, the "background" is not as simple to acquire and remove from the data. Background due to instrument noise is one type of background that we would definitely like to remove from Pedemis data. But if the Rx array is at all moved off from a prior location, the instrument noise will change dramatically mainly because the Tx coils are so close to the receivers. These Tx could can act like targets themselves, but their influence in the EMI data is considered instrument noise and is undesirable.

Our plan to remove this noise could center on simply taking thousands of measurements and interpolating between them in the 6-space consisting of Pedemis's 3D location in space and its current 3 Euler angles. Not only is that laborious, but trying to get that many measurements, including in the 2 meters outside the Tx array could take years even on an automated platform like the ERDC test stand.

Instead, we plan to reproduce the response (AKA instrument noise or instrument background) from the Tx coils using an equivalent source approach similar to the NSMS method. These equivalent sources will be found from a much smaller set of normal background measurements at known locations. Once this set of sources is known, the time domain response from the coils (as represented by the sources) can be quickly calculated anywhere in space. The location of the Rx array will be known from the Pedemis beacon type positioning as described in Sec. 3.3. Any future background type measurements in the air will be added to the training routine for the equivalent sources and their accuracy will be improved. This instrument background subtraction routine will be built into Pedemis so that any data collected by Pedemis will have this instrument noise removed before recording the data. Note that this solution for this instrument noise does not address the issue of gelogical noise in the EMI due to the soil.

3.5 Pedemis Operation Protocol

There will be several data collection protocols for using Pedemis depending on whether Pedemis will be used for detection and cued interrogation, and what the data quality is over each target. If Pedemis is to be used for the detection segment of the survey, then Pedemis is put into detection mode (see below for mode descriptions) until an anomaly is detected. Once detected, Pedemis is the placed over the anomaly, and data is acquired in cued interrogation mode #1. After this data is collected, a determination is made whether Pedemis should either 1) enter interrogation mode #2 (for widespread multiple targets) or #3 (for deep targets) or data collection over this anomaly should conclude.

Pedemis will have the following data collection protocols:

- **Detection Mode –** Data is acquired at 10 samples per second as Pedemis is transported over the ground. A plot of the z-component of the magnetic field will be displayed in real time on controlling device to facilitate anomaly detection. The Rx array is centered on the Tx array and fixed in position.

- **Cued Interrogation Mode #1 –** This mode directly follows a detection. Pedemis is set down centered over the anomaly with the Rx array still fixed in position. A static data shot using all nine Tx coils and all 9 receivers in this configuration is then taken. This data shot will take around 30 seconds. Depending on the results of this data, users will follow one of the following three courses of action:

  1. *Enter Cued Interrogation Mode #2*
  2. *Enter Cued Interrogation Mode #3*
  3. *Resume Detection Mode*

- **Cued Interrogation Mode #2 (for multiple and/or widespread targets) –** Based on the data from cued interrogation mode #1 using the JD method, a determination will be made (at first by expert users, later by computer algorithm) whether there are multiple and/or widespread targets in the field of view of Pedemis. If this is the case, then this interrogation mode is used. In this mode, the Rx array is positioned near each of the four corners of the Tx array in sequence (see the sketch in Fig. 3.16) for four 30 second data shots. Total time for this interrogation will be about 2 minutes. This mode provides an equivalent 6x6 array of vector magnetic field values from 9 independent transmitters over a 1.2m square area. These four positions avoid the Tx coils as much as possible (3.5cm smallest lateral separation) while yielding a uniform 6x6 composite data shot.

- **Cued Interrogation Mode #3 (for deep targets) –** This cued interrogation mode is used if deep targets seem to be present, but the data is not of sufficient SNR to make a reliable classification of the target. For this mode, the Rx array is left in the center of the Tx array (as in detection and cued #1 modes), but a longer data shot is acquired in order to integrate more samples and thus increase SNR for deep targets. This data shot may take up to 5 minutes to complete depending on the desired SNR.

During MR-1712, the determination of which data protocol to follow will be made by expert users, however we hope to be able to systematize the decision process into computer algorithms in future Pedemis work.

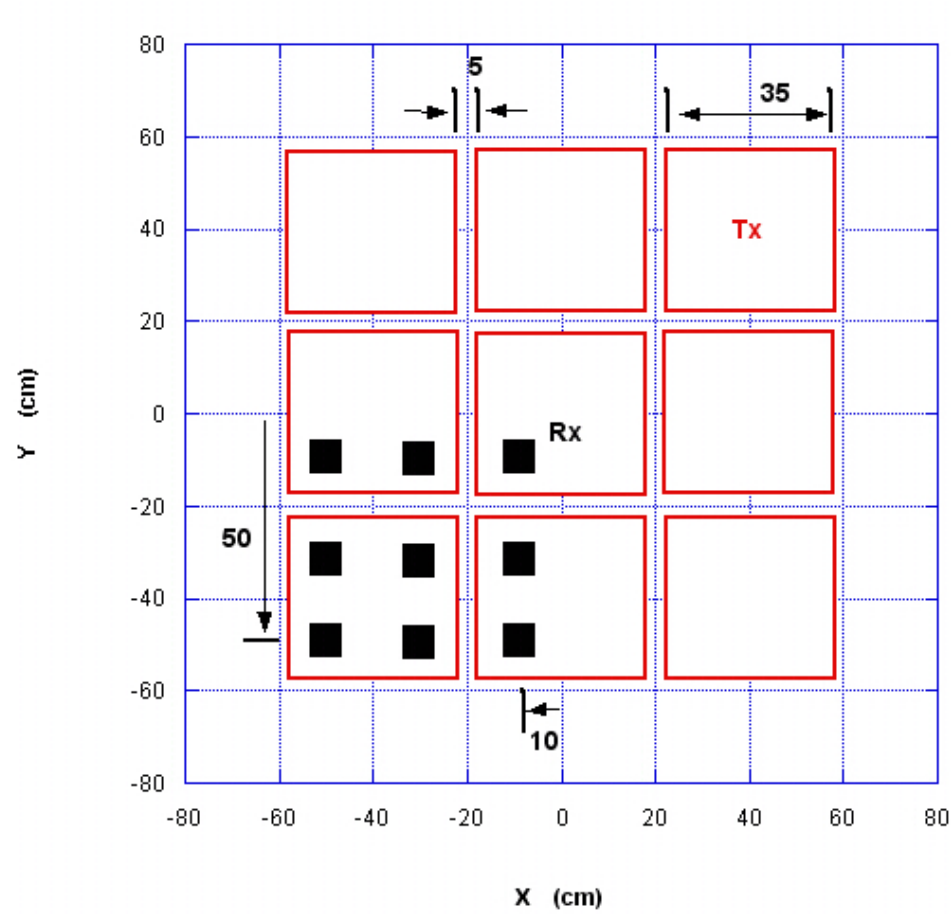

Figure 3.16: Pedemis DAQ Position #1 sketch. 35cm transmitters with 5cm spacing. The 50cm Rx array is shown in the lower left quadrant (AKA position "#1" of 4). These four positions avoid the Tx coils as much as possible while yielding a uniform 6x6 composite data shot.

4 Results and Discussion

4.1 Pedemis Hardware and Fabrication

As of January, 2012, the Tx and Rx arrays have arrays have been fabricated as shown in Figs. 3.2–3.4. The combined weight of these arrays is about 38 pounds which does not include cabling or gurney poles. The Tx array is 1.2 meters on a side, while the Rx array is 50cm on a side. The overall weight of the controlling electronics (NI cRIO) plus batteries is approximately 20 pounds.

The control electronics, the NI cRIO platform described in Sec. 3.2.c, have been acquired and shown to perform well given the prototype stage of the control software described in Sec. 4.2. The cables for Pedemis need to be constructed and connected to the Tx and Rx arrays.

As part of the Pedemis project, G&G Sciences has had enough funding to perform a critical redesign on the both the transmitter control board and the anti-aliasing filter board. The transmitter control board currently handles only up to 3 transmitters at once and is outdated in other ways. This board will be redesigned and constructed to have 9 transmitters on a single board, thus saving weight and complexity. In addition, the anti-aliasing filter board will also be redesigned to accom-

modate more channels and to use updated components. These upgraded circuit boards will benefit other current and future projects which use G&G Sciences hardware.

We still need to decide on what GPS to use with Pedemis and how exactly to broadcast the webpage.

4.2 Pedemis DAQ Control Software

At the Partners in Environmental Technology Symposium hosted by SERDP and ESTCP in Washington DC in November 2011, one of the main comments from industry who worked with the MetalMapper was that the interface was difficult to use. One reason for this was the jump from the software being used by the programmer (David George) to being used by those who didn't write the software and weren't used to all the particulars associated with digital geophysical mapping with advanced EMI instruments. These comments underscored the need for simple to use yet powerful software to control advanced EMI instruments like Pedemis.

Our goal with the Pedemis control software in written in LabVIEW is to program such a robust, powerful, simple, yet flexible and intuitive interface based on the web browser concept of tabs for different functionality. For example, one tab or window of the browser would be dedicated to configuring data acquisition parameters for Pedemis. This tab would be available, but rarely used in the field. Another tab would display information regarding the current or next anomaly and would have a simple button for data collection, a comment box, and a field plot for checking proper operation of the receivers. Yet another tab could be for a more in depth analysis of the current data using techniques such as JD or a Gauss Newton multiple dipole search [1]. Any nearby web enabled device should be able to connect to and control Pedemis, from a smart phone to an iPad, to a laptop computer.

The cRIO-9022 controller communicates with the cRIO-9116 FPGA chassis both controlling it and receiving data from the modules. This RT controller will also host this webserver described above. Most of the calculations and higher level operations are controlled on the RT controller while the FPGA mainly specializes in collecting the data itself. Figure 4.1 shows part of the Virtual Instrument (VI) which runs on the RT controller.

The NI-9222 modules collect data from 4 channels at 500KS/s which is sufficient for the time bands we are interested in with Pedemis (100μs to 25ms). Seven of these modules are needed due to the 27 receiver channels from the nine triaxial receiver cubes, and another channel monitors the transmitter current. The core function of the VI that runs on the cRIO-9116 FPGA chassis can be seen in Fig. 4.2.

Both the RT VI in Fig. 4.1 and the FPGA VI in Fig. 4.2 have what's referred to as a "front panel" that displays the information associated with each VI. The prototype front panel for the data collection reported in Sec. 4.3 performed with only minimum functionality, but was sufficient for acquiring data from Pedemis's 9 transmitters. This interface will be continually improved throughout the remainder of this project and throughout any follow-on work.

4.3 Initial Data, November 2011

We were able to collect initial proof of concept data outside of G&G Sciences office in Grand Junction, CO in November, 2011. Pedemis was not fully fabricated, and the main difference between the hardware used to collect these data and the finished instrument are as follows:

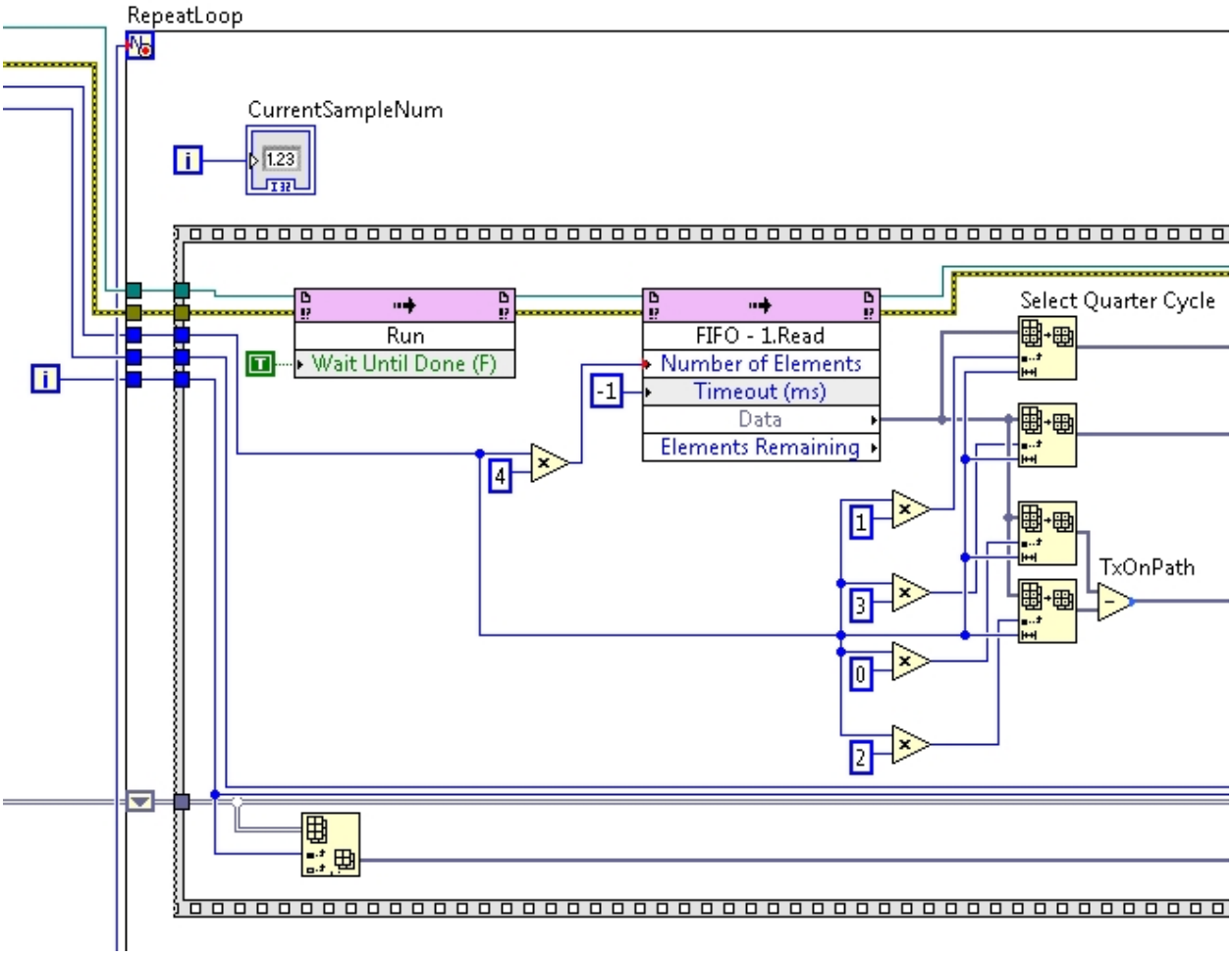

Figure 4.1: Partial view of Pedemis RT control software. This VI manages file I/O, runs the webserver, performs the averaging and data analysis, and controls most all functions except actual data collection itself which is handled on the cRIO-9116 FPGA chassis.

1. **Tx array –** The individual Tx coils were fabricated for this initial data, but the associated cabling had not been. As a result, we had to manually hook up each transmitter during data collection. As another result, because these coils were open circuit (if not the one being energized), they tended to have a longer than usual secondary z-component response for the receivers. Thus, the z-component of the received field is noisier than the x or y components in this initial data.

2. **Rx array –** The Rx array was fabricated, but the cabling to hook it up to the cRIO DAQ was not complete. Instead, we used the 5 receiver cubes and associated cabling of the MPV2 for this initial data. The MPV2 Rx cubes are the same design as the Pedemis cubes, so these preliminary results should be very similar to the production data once Pedemis is fully fabricated.

3. **Transmitter Control Board –** As mentioned in Sec. 4.1, the transmitter control board will be redesigned for Pedemis. For these initial data shots, we used the MPV2 transmitter control

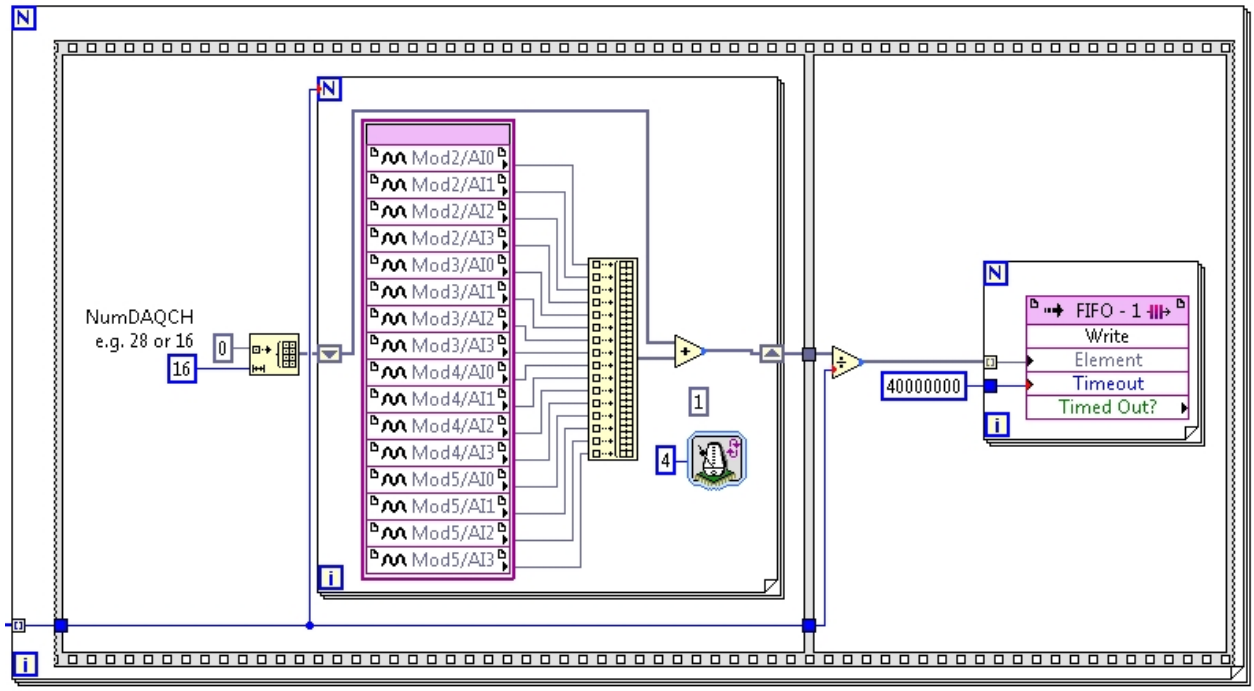

Figure 4.2: Pedemis FPGA control software. This VI

board.

4. **Analog Anti-aliasing Filters –** Likewise with the anti-aliasing filter boards, since these will be redesigned for Pedemis, we used the MPV2 board.

We did use the cRIO based system with the LabVIEW VIs described in Sec. 4.2 to control the boards and sample the output of the Rx channels after the filter board (see Fig. 4.1). The core functionality of these VIs will be improved during the remainder of the project, but the core control logic is complete.

Figure 4.3 show the data acquisition setup and process at Grand Junction, CO in November, 2011. Data was collected (a "shot") at 5 MPV2 positions over the Tx array with all 9 transmitters firing in turn. In terms of orientation, the MPV2 handle is pointing in the negative y direction. Four total data shots were collected:

1. A background shot

2. A shot over a 4 inch steel sphere. The sphere was located at depth 26 cm (to nearest point on sphere) under the corners of the four upper left transmitters.

3. Positioning test shot with no target. For this shot, the MPV2 sensor head was left in one location (at the bottom right corner of the Tx array) while all nine transmitters fired in turn. This was to test the positioning algorithms in Sec. 3.3 with no target present.

4. Positioning test shot with no target. This time, the MPV2 sensor head was outside the Tx array to the left.

Figure 4.3: Initial data setup in Grand Junction CO in November, 2011. The MPV2 receivers were used as the Pedemis Rx cabling was incomplete.

The initial data was analyzed for satisfactory SNR and reasonableness in our lab. Figure 4.4 shows the raw data from the 5 MPV2 receivers situated in the top left corner of the Tx array and the center transmitter firing. As expected, the z-components of the received magnetic field are more noisy than the x or y components due to the open terminals at the remaining transmitter terminals. Note that we integrated and averaged one hundred 10Hz measurements for these data. Using our Gauss-Newton dipole inversion routine [1], we get the polarizabilities shown in Fig. 4.5 using only the x and y components of the received magnetic field.

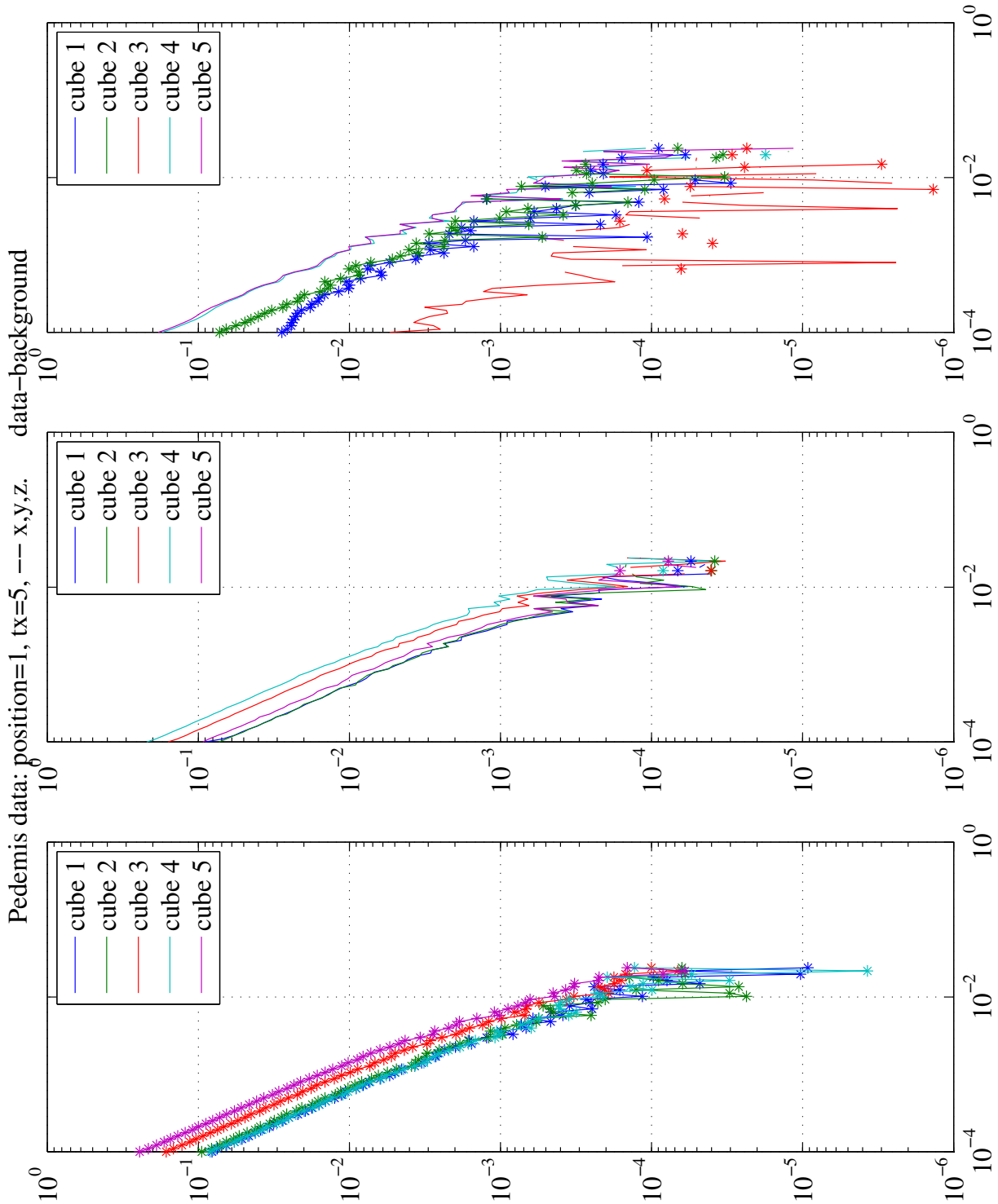

Figure 4.4: Example data from Pedemis. Raw data from the 5 MPV2 receivers situated in the top left corner of the Tx array and the center transmitter firing. The lower subfigure shows the x-component, the center subfigure shows the y-component, and the upper subfigure shows the z-component.

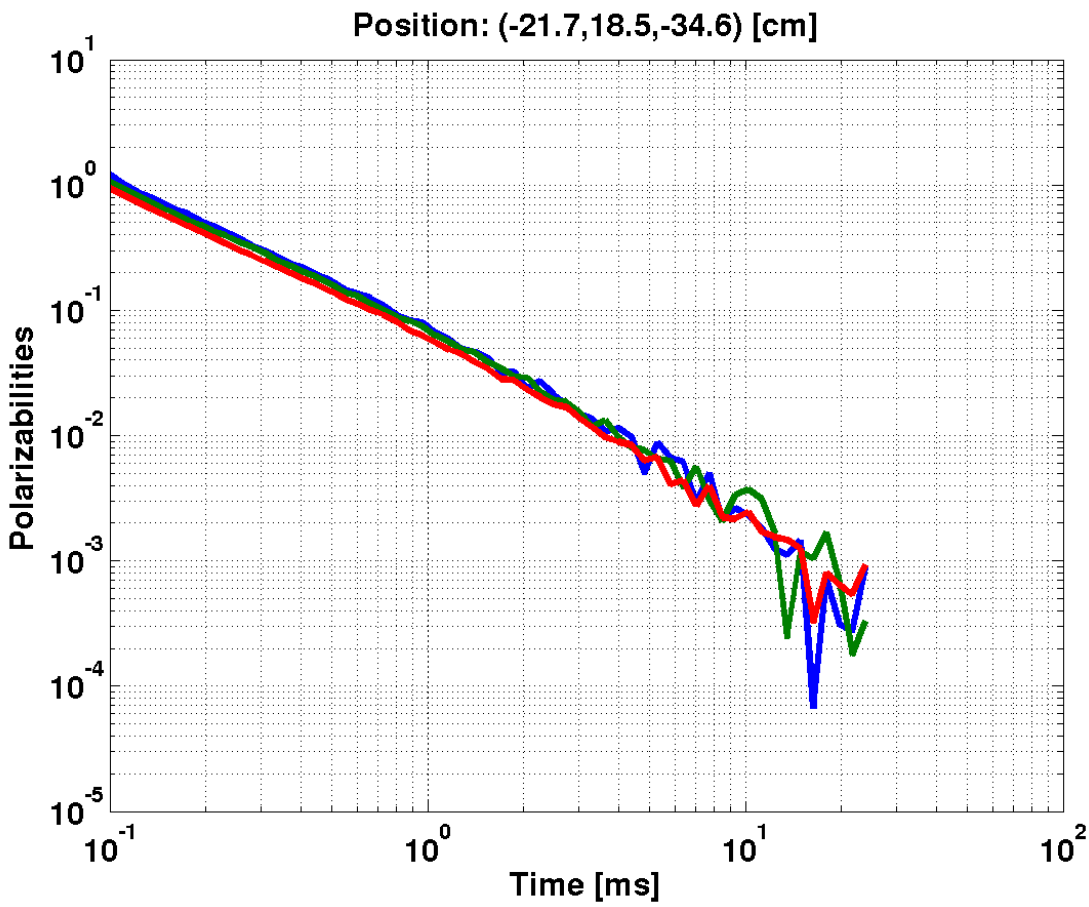

Figure 4.5: Polarizabilities from data in Fig. 4.4. These were calculated using only the x and y components of the received magnetic field due to the z-component being noisy (see discussion above).

5 Conclusions to Date

SERDP project MR-1712 entitled "Portable Electromagnetic Induction Sensor with Integrated Positioning" is slightly more than halfway complete. A delay of a few months has developed due to the other commitments of G&G Sciences. However, the remaining fabrication should be completed by the end of April, 2012. The Tx and Rx assemblies are designed and fabricated. The DAQ electronics consists of the National NI cRIO platform which is much lighter and more efficient that prior DAQ platforms. Software to control the cRIO DAQ process has been written in NI's LabVIEW. This software has been used to successfully acquire data initial over a sphere as shown in Sec. 4.3. Inversion of the data acquired during these initial tests has yielded satisfactory polarizabilities of the spherical target. In addition, precise positioning of the Rx assembly has been achieved via position inversion algorithms based solely on the data acquired from the receivers during the "on-time" of the primary field (see Sec. 3.3).

Major tasks still to complete included redesigning and integrated new transmitter and filter board control circuitry as well as final cable construction and integration. The LabVIEW programs must also be matured to become more user friendly. A more extensive prove-out is scheduled for May, 2012 after which will follow an extensive data analysis. Finally, we intend to go to Aberdeen Proving Ground in the Fall of 2012.

References

[1] Tomasz M. Grzegorczyk, Benjamin E. Barrowes, Fridon Shubitidze, Juan Pablo Fernandez, and Kevin O'Neill. Simultaneous identification of multiple unexploded ordnance using electromagnetic induction sensors. IEEE Transactions on Geoscience and Remote Sensing, 2011. ISSN 01962892. URL http://dx.doi.org/10.1109/TGRS.2011.2108302. 3, 23, 26

[2] Fridon Shubitidze, Juan Fernndez, Irma Shamatava, Benjamin Barrowes, and Kevin O'Neill. Joint diagonalization applied to the detection and discrimination of unexploded ordnance. Geophysics, submitted for publication. 3

[3] Fridon Shubitidze, Ben Barrowes, Irma Shamatava, Juano Pablo Fernndez, and Kevin O'Neill. The ortho normalized volume magnetic source technique applied to live-site uxo data: Inversion and classification studies. SEG Special Issue, September 2011. 3

[4] F. Shubitidze, D. Karkashadze, J. P. Fernandez, B. E. Barrowes, K. O'Neill, Grzegorczyk, and I. Shamatava. Applying a volume dipole distribution model to next-generation sensor data for multi-object data inversion and discrimination. Detection and Sensing of Mines, Explosive Objects, and Obscured Targets Xv, 7664, 2010. doi: 10.1117/12.850651. 3

[5] F. Shubitidze, B. Barrowes, J. P. Fernández, and K. O'Neill. Combined NSMC and Pseudo-Spectral Finite-Difference Method for Inverting a Buried Object Location. Symposium on the Application of Geophysics to Engineering and Environmental Problems, 2007 . 3

[6] F. Shubitidze, B. Barrowes, J. P. Fernández, Irma Shamatava, and K. O'Neill. NSMC for UXO discrimination in cases with overlapping signatures. SPIE, 2007. 3

[7] F. Shubitidze, B. E. Barrowes, K. O'Neill, I. Shamatava, K. Sun, and K.D. Paulsen. Total normalized surface magnetic charge for UXO discrimination. NATO Advanced Study Institute "Imaging for Detection and Identification", 23 July–5 August 2006. Ciocco, Italy. 3

[8] F. Shubitidze, B. Barrowes, and K. O'Neill. Normalized surface magnetic charge for UXO discrimination: multiple objects. SERDP Partners Symposium, November 2006. Poster. 3

[9] F. Shubitidze, K. O'Neill, B. Barrowes, J. P. Fernández, I. Shamatava, K. Sun, and K.D. Paulsen. Application of the normalized surface magnetic charge model to UXO discrimination in cases with overlapping signals. J. Appl. Geophys., 61(3-4): 292–303, Mar. 2007. 3

[10] F. Shubitidze, K. O'Neill, I. Shamatava, K. Sun, , and K. D. Paulsen. Total magnetic charge for fast screening of highly contaminated UXO sites. In proceedings of 2005 IEEE international symposium on Antennas and Propagation and USNC/CN/URSI North American Radio Science meeting, on CD, 2005. 3

[11] F. Shubitidze, K. O'Neill, I. Shamatava, K. Sun, and K.D. Paulsen. Total magnetic charge for fast screening of highly contaminated UXO sites. 2005 IEEE Antennas and Propagation Society International Symposium (IEEE Cat. No. 05CH37629), vol. 3A:856 – 9, 2005. 3

[12] Fridon Shubitidze, Kevin O'Neill, Irma Shamatava, Keli Sun, and Keith Paulsen. Combined differential evolution and surface magnetic charge model algorithm for discrimination of UXO from non-UXO items: Simple and general inversions. Proceedings of SPIE - The International Society for Optical Engineering, 5794(Part I):346 – 357, 2005. ISSN 0277-786X. 3

[13] L. R. Pasion. A unified approach to uxo discrimination using the method of auxiliary sources. Technical report, 2006. 3

[14] B. E. Barrowes, K. O'Neill, T. M. Grzegorczyk, X. Chen, and J. A. Kong. Broadband analytical magnetoquasistatic electromagnetic induction solution for a conducting and permeable spheroid. IEEE Trans. on Geoscience and Remote Sensing, 42 (11):2479–2489, 2004. 3

[15] B. E. Barrowes, K. O'Neill, T. M. Grzegorczyk, and J. A. Kong. On the asymptotic expansion of the spheroidal wave function and its eigenvalues for complex size parameter. Studies in Applied Mathematics, 113(3):271–301, Oct. 2004. 3

[16] Chi On Ao, Henning Braunisch, Kevin O'Neill, and Jin Au Kong. Quasi-magnetostatic solution for a conducting and permeable spheroid with arbitrary excitation. IEEE Trans. Geosci. Remote Sensing, 40:887–897, Apr. 2002. 3

[17] Henning Braunisch, Chi On Ao, Kevin O'Neill, and Jin Au Kong. Magnetoquasistatic response of conducting and permeable prolate spheroid under axial excitation. IEEE Trans. Geosci. Remote Sensing, 39:2689–2701, Dec. 2001. 3

[18] X. Chen, K. O'Neill, B. E. Barrowes, T. M. Grzegorczyk, , and Jin Au Kong. Application of a spheroidal mode approach with differential evolution in inversion of magneto-quasistatic data for UXO discrimination. Inverse Problems, 20(6):27–40, 2004. 3

[19] F. Shubitidze, K. O'Neill, K. Sun, and I. Shamatava. Application of broadband EMI responses to infer buried object's aspect ratio. International Geoscience and Remote Sensing Symposium (IGARSS), 3:1542 – 1545, 2002. 3

[20] Benjamin E. Barrowes, Kevin O'Neill, Tomasz M. Grzegorczyk, and J. A. Kong. Broadband, Analytic Electromagnetic Induction (EMI) Response from Spheroidal Objects for Arbitrary Excitation. Progress in Electromagnetics Research Symposium (PIERS), October 2003. 3

[21] Juan Pablo Fernandez, Benjamin Barrowes, Alex Bijamov, Tomasz Grzegorczyk, Nicolas Lhomme, Kevin O'Neill, Irma Shamatava, and Fridon Shubitidze. MPV-II: an enhanced vector man-portable emi sensor for uxo identification. volume 8017, page 801707. SPIE, 2011. doi: 10.1117/12.884085. URL http://link.aip.org/link/?PSI/8017/801707/1. 5, 11

[22] F. Shubitidze, B. Barrowes, I. Shamatava, J. P. Fernández, and K. O'Neill. Combining NSMC and High Quality MPV-TD Data for UXO Discrimination. Proc. IEEE Int. Geosci. Remote Sensing Symp. (IGARSS), 2008. 5, 11

[23] Fridon Shubitidze, Juan Pablo Fernández, Benjamin E. Barrowes, Irma Shamatava, and Kevin O'Neill. Normalized Surface Magnetic Source model applied to Camp Sibert data. In Applied Computational Electromagnetics Symposium (ACES), Monterey, CA, Mar. 2009. 5

[24] W. M. Wynn, C. P. Frahm, P. J. Carroll, R. H. Clark, J. Wellhoner, and M. J. Wynn. Advanced superconducting gradiometer/magnetometer arrays and a novel signal processing technique. IEEE Transactions on Magnetics, MAG-11(2):701 – 707, 1975. URL http://dx.doi.org/10.1109/TMAG.1975.1058672. 5